Translational Oncology 14 (2021) 100888

Contents lists available at ScienceDirect

Translational Oncology

journal homepage: www.elsevier.com/locate/tranon

Classification of gastric cancers based on immunogenomic profiling

Zhixian Liu [a,c], Zehang Jiang [b,c], Nan Wu [a], Guoren Zhou [a,*], Xiaosheng Wang [c,**]

[a] The Affiliated Cancer Hospital of Nanjing Medical University, Jiangsu Institute of Cancer Research, Jiangsu Cancer Hospital, 42 Baiziting, Nanjing 210009, Jiangsu, China
[b] State Key Laboratory of Ophthalmology, Zhongshan Ophthalmic Center, Sun Yat-sen University, Guangzhou, 500040, Guangdong, China
[c] Biomedical Informatics Research Lab, School of Basic Medicine and Clinical Pharmacy, China Pharmaceutical University, Nanjing 211198, Jiangsu, China

ARTICLE INFO

Article history:
Received 18 June 2020
Received in revised form 3 September 2020
Accepted 21 September 2020

ABSTRACT

Background: Extensive evidence showed that gastric cancer (GC) is heterogeneous, and many studies have been focused on identifying GC subtypes based on genomic profiles. However, few studies have specifically explored the GC classification and predicted the classification accuracy that may help facilitate the optimal stratification of GC patients responsive to immunotherapy.

Methods: Using two publicly available GC genomics datasets, we classified GC on the basis of 797 immune related genes. Unsupervised and supervised machine learning methods were used to predict the classification.

Results: We identified two GC subtypes that we named as Immunity-High (IM-H) and Immunity- Low (IM-L), and demonstrated that this classification was duplicable and predictable by analyzing other datasets. IM-H subtype was characterized by greater immune cell infiltration, stronger immune activities, lower tumor purity, as well as worse survival prognosis compared to IM-L subtype. Besides the immune signatures, some cancer-associated pathways were hyperactivated in IM-H, including TGF-beta signaling pathway, Focal adhesion, Cell adhesion molecules (CAMs), Calcium signaling pathway, mTOR signaling pathway, MAPK signaling pathway and Wnt signaling pathway. In contrast, IM-L presented depressed immune signatures and increased activation of base excision repair, DNA replication, homologous recombination, non-homologous end-joining and nucleotide excision repair pathways. Furthermore, we identified subtype-specific genomic or clinical features, and subtype-specific gene ontology and networks in IM-H and IM-L subtype.

Conclusions: We proposed and validated two reproducible immune molecular subtypes of GC, which has potential clinical implications for GC patient selection of immunotherapy.

Introduction

Gastric cancer (GC) is one of the most common malignant tumors and the third leading cause of cancer-related death worldwide [1]. GC is common in Asian countries, especially in China [2]. Based on the molecular characteristics of genomic profiles, The Cancer Genome Atlas (TCGA) classified GC into four subtypes: Epstein–Barr virus (EBV) associated, microsatellite instable (MSI), genomically stable (GS), and chromosomal instability (CIN) [3]. The Asian Cancer Research Group (ACRG) classified GC into four subtypes: microsatellite stable (MSS)/epithelial-mesenchymal transition (EMT), MSI, MSS/p53+, and MSS/p53 inactive [4]. Abundant evidence showed that GC treatment faces enormous challenges as its high heterogeneity [5]. Zhou et al. identified a novel classification of GC microenvironment, which comprised three robust non-negative matrix factorization (NMF) based clusters with active, suppressive, and lacking immune responses, which exhibited a strong prognostic value [6]. Zeng et al. defined three GC subgroups based on a tumor microenvironment score (TME) score, which included three immunity clusters whose immune module gene signatures interpreted the response of gastric tumors to immunotherapies [7]. These previous efforts to classify GC might provide the basis for developing targeted therapies for GC.

Recently, tumor immunotherapy has been successful in treating various malignant tumors [8]. Particularly, the immune checkpoints blockade has achieved great success in clinical malignant tumor treatment [9]. Immune checkpoint inhibitors targeting CTLA4, PD1, or PD-L1 blockade is being assessed in the GC immunotherapy. FDA has approved the PD1 inhibitor pembrolizumab to treat advanced malignancies with deficient mismatch repair (dMMR, or MSI) including the MSI subtype of GC. Thus, it is necessary to consider immunotherapy for GC, as the treatment options for GC are quite limited. Unfortunately, immunotherapeutic strategies are only beneficial to less than 20% of cancer patients [10]. This suggests that not all GC patients have response to immunotherapy. However, certain

* Correspondence to: G. Zhou, The Affiliated Cancer Hospital of Nanjing Medical University, Jiangsu Institute of Cancer Research, Jiangsu Cancer Hospital, 42 Baiziting, Nanjing 210009, Jiangsu, China
** Correspondence to: X. Wang, Biomedical Informatics Research Lab, School of Basic Medicine and Clinical Pharmacy, China Pharmaceutical University, Nanjing 211198, Jiangsu, China
E-mail addresses: zhouguoren888@163.com, (G. Zhou), xiaosheng.wang@cpu.edu.cn. (X. Wang).

http://dx.doi.org/10.1016/j.tranon.2020.100888

genomic features, such as tumor mutation burden (TMB) or neoantigen load, *PD-L1* expression, and deficient DNA mismatch repair, have been reported to associate with cancer immunotherapeutic responsiveness [11–15].

In this study, we classified GC into two distinct subtypes by immunogenomic profiling: IM-H and IM-L. We demonstrated the stability and reproducibility of this classification in three independent largescale datasets by a deep learning approach. Furthermore, we identified the subtype-specific clinical features and molecular characters, including genes, gene ontology, tumor mutation load (TMB), copy number alterations, pathways, and networks. The identification of immune signature-associated GC subtypes may facilitate the optimal selection of GC patients responsive to immunotherapy.

Materials and methods

Materials

We downloaded TCGA stomach cancer (STAD) RNA-seq gene expression profiles (Level 3), gene somatic mutation matrix (Level 3), somatic copy number segments (germline CNV removed) and clinical phenotype data, from UCSC Xena browser (https://xenabrowser.net/datapages/). The Asian Cancer Research Group (ACRG) dataset were obtained from Gene Expression Omnibus (GEO) (GSE62254). We also download an additional Singapore patient cohort from GEO (GSE15459) as testing set for machine learning (see below).

Univariate Cox proportional hazards (Coxph) regression

Based on the Coxph regression model, we applied a univariate risk analysis on 797 immune genes [16] to assess the risk of these genes in GCs, and extracted the hazard ratio (HR) and *P* value, where HR > 1 was considered as a higher risk, HR < 1 as a low risk. Then we used R package "survminer" to visualize the Coxph results.

Unsupervised clustering

We used hierarchical clustering to divided GCs for TCGA and ACRG datasets based on the 160 immune genes. The clustering results are obtained by calculating the euclidean distance. Eventually, GC patients were divided into high immunogenicity (IM-H) and low immunogenicity (IM-L) substitutions.

Survival analysis

We compared overall survival (OS) and disease-free survival (DFS) time between two groups of GC patients divided by the cluster results (IM-H versus IM-L) or gene expression levels. Kaplan-Meier survival curves were used to exhibit the survival differences between two groups of patients. Gene expressions above or below the median values were divided into two groups. The log-rank test was used to evaluate the significance of survival-time differences with a threshold of $P < 0.05$.

Evaluation of immune cell infiltration degree and stromal content in GC.

ESTIMATE [17] was used to quantify immune infiltration and stromal levels to compare the overall immune cell infiltration level and stromal components between two groups of GC patients. In addition, we used TIMER [18] and CIBERSORT [19] tools to analyze the 6 major immune cells (B cells, CD4 + T cells, CD8 + T cells, neutrophils, macrophages and DC cells) and calculate the proportions of 22 human leukocyte cell subsets and compared the proportions of the leukocyte cell subsets in each GC sample.

Evaluation of tumor purity, tumor aneuploid and TMB

ABSOLUTE [20] and ASCAT [21] algorithm were used to evaluate tumor purity and aneuploidy levels in TCGA and ACRG dataset. Each sample finally received a tumor purity score and aneuploid quantitative score. For each tumor sample, we determined its TMB as the total count of somatic mutations detected in the tumor. We compared the differences in purity and heteroploidy between IM-H and IM-L using the Mann–Whitney *U* test.

Gene-set enrichment analysis

We used GSEA software [22] to identify significantly pathways which were activated in IM-H and IM-L subtype based on 186 KEGG gene sets with the threshold of FDR < 0.1. Gene sets with less than 10 genes were filtered out. The common pathways identified in both datasets were selected.

Somatic copy number alteration (SCNA) analysis

GISTIC2.0 [23] was applied to analyze copy number levels in TCGA. All params were set as default except the "armpeel" were set to 1. We eventually obtained the copy number variation levels of each gene in each sample (0 indicates no change in copy number, > 0 indicates copy number amplification, < 0 indicates copy number deletion).

Weighted correlation network analysis

WGCNA [24] was used to identify the gene modules (gene ontology) which were highly correlated with immune cell infiltration. We performed preliminary filtering for genes with variance less than the 1/8 quantile, then we got the best soft threshold value of 3 after "powerEstimate", and "minModuleSize" was set to 50 to filter out the modules with low correlation. Finally we got the correlation heat map between gene modules and the trait. We imported the highest correlation module to Cytoscape (https://cytoscape.org/) to visualize the module network and find the hub genes of the module. The ClueGO [25] and CluePedia [26] plug-ins were used to analyze the relevant pathways in the module.

Deep neural network (DNN) predicts classification accuracy

To verify the accuracy of the classification results, we treat TCGA GCs as the deep neural network training set, while ACRG and GSE15459 as the testing set. We used the R package "TDM" [27] to standardize the mRNA data of different platforms to make RNA-seq and microarray data comparable. Those 160 immune-risk related genes were then standardized as [28]:

$$v_{rank} = \frac{1}{n}.(\ rank(v_1), \ldots,\ rank(v_n))$$

Then, we set the loss function as the cross-entropy loss function (cross entropy):

$$L(\hat{y}, y) = -\hat{y}\ log(y) - (1-\hat{y})\ log(1-y)$$

$\hat{y}$ was the predicted value of the model, and y was the true value of the training set.

The random forest model and the Naive Bayes model in Weka (https://www.cs.waikato.ac.nz/ml/) library was used to classify the GC subtypes. We applied the Python Keras library (https://github.com/fchollet/keras) to train and predict the deep neural network model.

Results

Landscape of the immune microenvironment phenotypes in GCs

We first applied a risk analysis on 797 immune genes and found that 160 immune genes in TCGA were significantly associated with risk and

more than half of the 160 risk-associated genes were significantly related with the risk in ACRG (Supplementary materials, Table S1). Based on these 160 immune genes expression level, we hierarchically-clustered GC in two datasets (TCGA and ACRG). Interestingly, both datasets showed similar clustering results, with two clusters being clearly separated. We defined the two clusters as: Immunity High (IM-H) and Immunity Low (IM-L) (Fig. 1A). Comparing the expression of risk-related genes in IM-H and IM-L in two datasets, we found that in TCGA, 146 of 160 (91%) risk-related genes highly expressed in IM-H subtype, 6 of 160 (4%) highly expressed in IM-L subtype, and in ACRG, 135 of 160 (85%) risk-related genes highly expressed in IM-H subtype, 10 of 160 (6%) highly expressed in IM-L subtype (student's *t*-test, FDR < 0.05, Fig. 1B). Moreover, the genes that are highly expressed in IM-H group are all high-risk genes (HR > 1) in both datasets, and five of the six related to low-risk genes are highly expressed in IM-L group (student's *t*-test, FDR < 0.05), including *EZH2*, *ITGB4*, *PHRF1*, *KLF5* and *BRIP1* (Fig. 1B).

Then we used ESTIMATE [17] to evaluate the immune cell infiltration level (immune score) and the matrix content level (stromal score) to compare the differences of tumor microenvironment between the IM-H and IM-L subtypes in the two datasets. We found that the immune score and the stromal score were significantly higher in IM-H than in IM-L in both datasets (Mann-Whitney *U* test, immune score: $P = 3.08e\text{-}31$ (TCGA), $P = 1.78e\text{-}16$ (ACRG); stromal score: $P = 3.40e\text{-}54$ (TCGA), $P = 3.27e\text{-}35$ (ACRG)) (Fig. 1C). When we used ABSOLUTE [20] and ASCAT [21] to evaluate tumor purity and tumor aneuploidy, the result showed IM-L subtype had higher tumor purity (Mann-Whitney U test, $P = 7.71e\text{-}3$ (TCGA), P

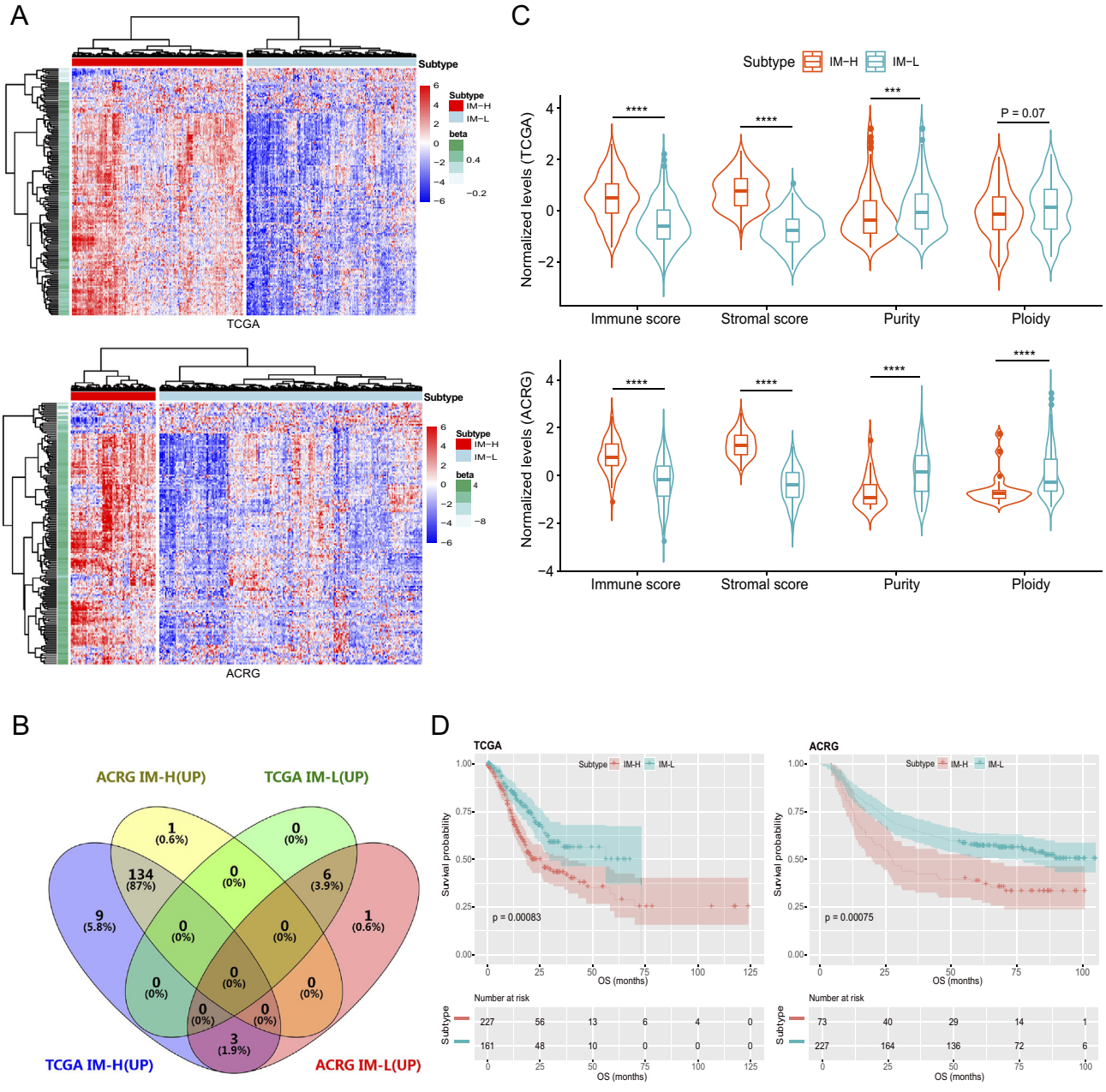

Fig. 1. Immune genomic analysis identified different subtypes in TCGA and ACRG, and showed different phenotypes. **A.** Heatmaps of hierarchical clustering of 160 risk genes identified two subtypes in TCGA and ACRG: Immunity-high (IM-H), Immunity-low (IM-L). The green bar on the left represents the risk regression β-value. β > 0 indicates a higher risk and β < 0 indicates a lower risk. **B.** The Venn diagram showed risk genes with high expression in IM-H and IM-L subtype in TCGA and ACRG. IM-H (UP) represents risk genes that are up-regulated in IM-H. IM-L (UP) represents risk genes that are up-regulated in IM-L. **C.** Comparison of the immune cell infiltration, stroma levels, tumor purity and tumor aneuploidy between GC subtypes. *: $P < 0.05$, **: $P < 0.01$, ***: $P < 0.001$, ****: $P < 0.0001$. **D.** Comparison of survival prognosis between IM-H and IM-L subtypes. (For interpretation of the references to colour in this figure legend, the reader is referred to the web version of this article.)

= 1.24e-4 (ACRG)) and aneuploidy (Mann-Whitney U test, $P = 0.07$ (TCGA), $P = 5.31e\text{-}5$ (ACRG)) than IM-H subtype (Fig. 1C). The above results indicated that IM-H subtype had higher immune cell infiltrate levels and matrix contents than IM-L subtype, while IM-L subtype had more tumor cells (higher tumor purity) than IM-H subtype.

In addition, survival analysis showed that these two subtypes had distinct clinical outcomes. The IM-H subtype likely had a worse prognosis and the IM-L subtype likely had a better prognosis (Fig. 1D), indicating that the degree of immune cell infiltration is negatively correlated with prognosis in GC.

IM-H had more active immune microenvironment compared to IM-L subtype

The tumor immune microenvironment is a complex dynamic system. Different immune microenvironment had different effects on the immunotherapy response in tumor patients. In order to clarify the differences of immune cells components in these two immune subtypes, we first compared the percentage of lymphocyte infiltration according to the TCGA GC pathological slides data, and found that IM-H subtype had markedly higher percentages of lymphocyte infiltration compared to IM-L (Mann-Whitney *U* test, $P = 0.04$, Fig. 2A). We then evaluated the differences of major immune cells by TIMER [18], and found that IM-H had much higher density of immune cells, such as B cells, CD4+ T cells, CD8+ T cells, neutrophil cells, macrophage cells and Dendritic cells (Fig. 2B, Supplementary materials, Table S2). Furthermore, we compared the proportions of 22 leukocyte cell subsets that were evaluated by CIBERSORT [23] between IM-H and IM-L, and found that IM-H harbored higher proportions of B cells naïve, B cells memory, T cells CD8, Monocytes, Macrophages M2, Mast cells resting (Mann-Whitney U test, FDR < 0.05;). In contrast, IM-L harbored higher proportions of Plasma cells, T cells CD4 memory resting, T cells follicular helper, T cells regulatory (Tregs), NK cells resting, NK cells activated, Macrophages M0, Mast cells activated (Mann-Whitney U test, FDR < 0.05; Fig. 2C, Supplementary materials, Table S3). This further demonstrates that IM-H are associated with stronger immune activity and more active immune microenvironment in GC. Intriguingly, M0 macrophages that incite inflammation had higher proportions in IM-L than in IM-H, while inflammation inhibiting M2 macrophages that also encourage tissue repair had higher proportions in IM-H. This finding indicates that the IM-L disease state promotes inflammatory infiltrates and depresses tissue repair compared to IM-H, which may promote invasion.

Identification of IM-H and IM-L subtype-specific pathways, genomic, clinical features, gene ontology, and networks

Identification of GC subtype-specific pathways

We used GSEA to identify a number of KEGG [29] pathways enriched in IM-H and IM-L. Typically, the immune-associated pathways were highly active in IM-H (Fig. 3A) and included Leukocyte transendothelial migration, ECM-receptor interaction, Fc gamma R-mediated phagocytosis, Chemokine signaling pathway, Hematopoietic cell lineage and Cytokine-cytokine receptor interaction. This result demonstrated the elevated immune activity in IM-H. Besides, we also identified various cancer-associated pathways that were hyperactivated in IM-H, including TGF-beta signaling pathway, Focal adhesion, Cell adhesion molecules (CAMs), Calcium signaling pathway, mTOR signaling pathway, MAPK signaling pathway and Wnt signaling pathway. This suggests that the activities of these cancer-associated pathways are positively related with GC immunity. In contrast, subtype IM-L was enriched in pathways related to Base excision repair, DNA replication, Homologous recombination, Non-homologous end-joining and Nucleotide excision repair (Fig. 3A), suggesting that the chromosome instability

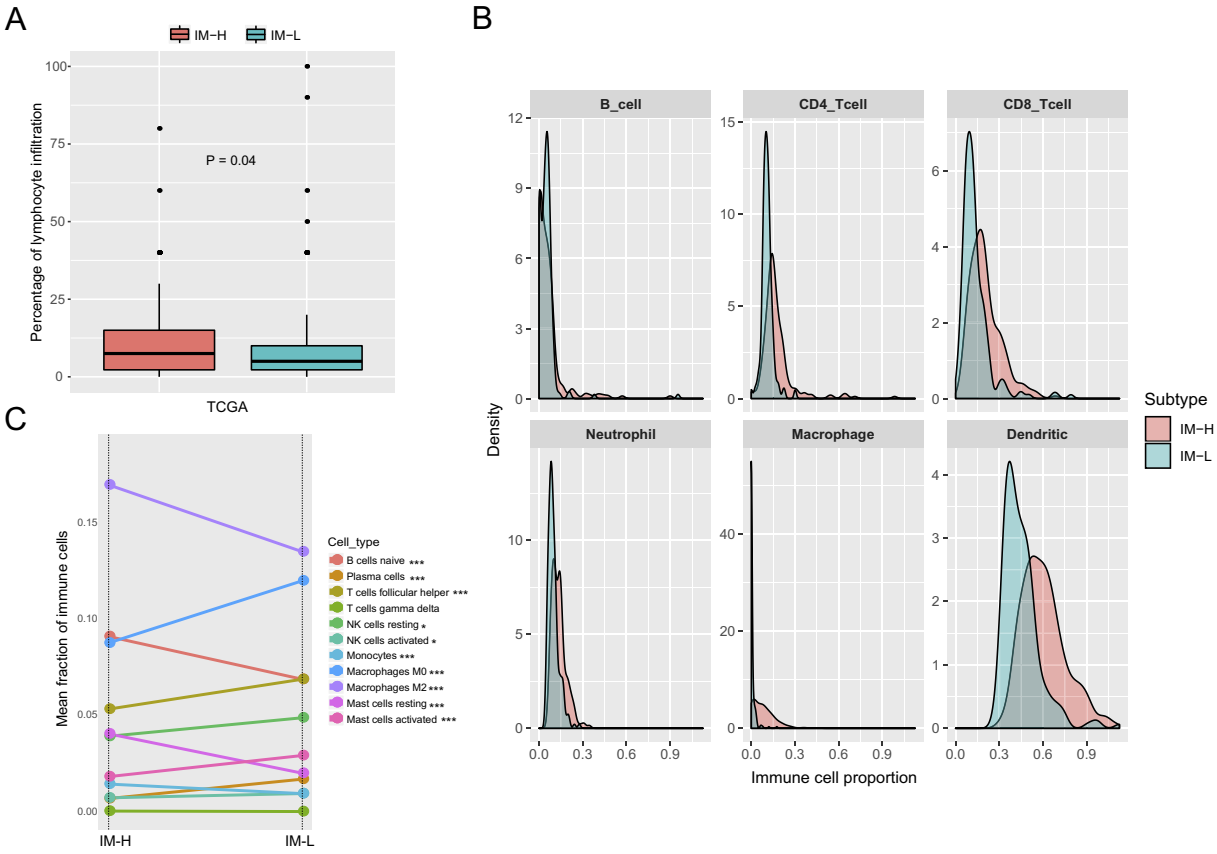

Fig. 2. Comparison of the proportions of immune cell subsets between GC subtypes. **A.** The TCGA GC pathological slides data show that IM-H GCs had markedly higher percent of lymphocyte infiltration than IM-L GCs. **B.** Comparison of abundance of six tumor-infiltrating immune cell types by TIMER between IM-H and IM-L GCs. **C.** IM-H GCs have significantly different leukocyte cell subset infiltrates estimated by CIBERSORT compared to IM-L GCs. *: P < 0.05, **: P < 0.01, ***: $P < 0.001$.

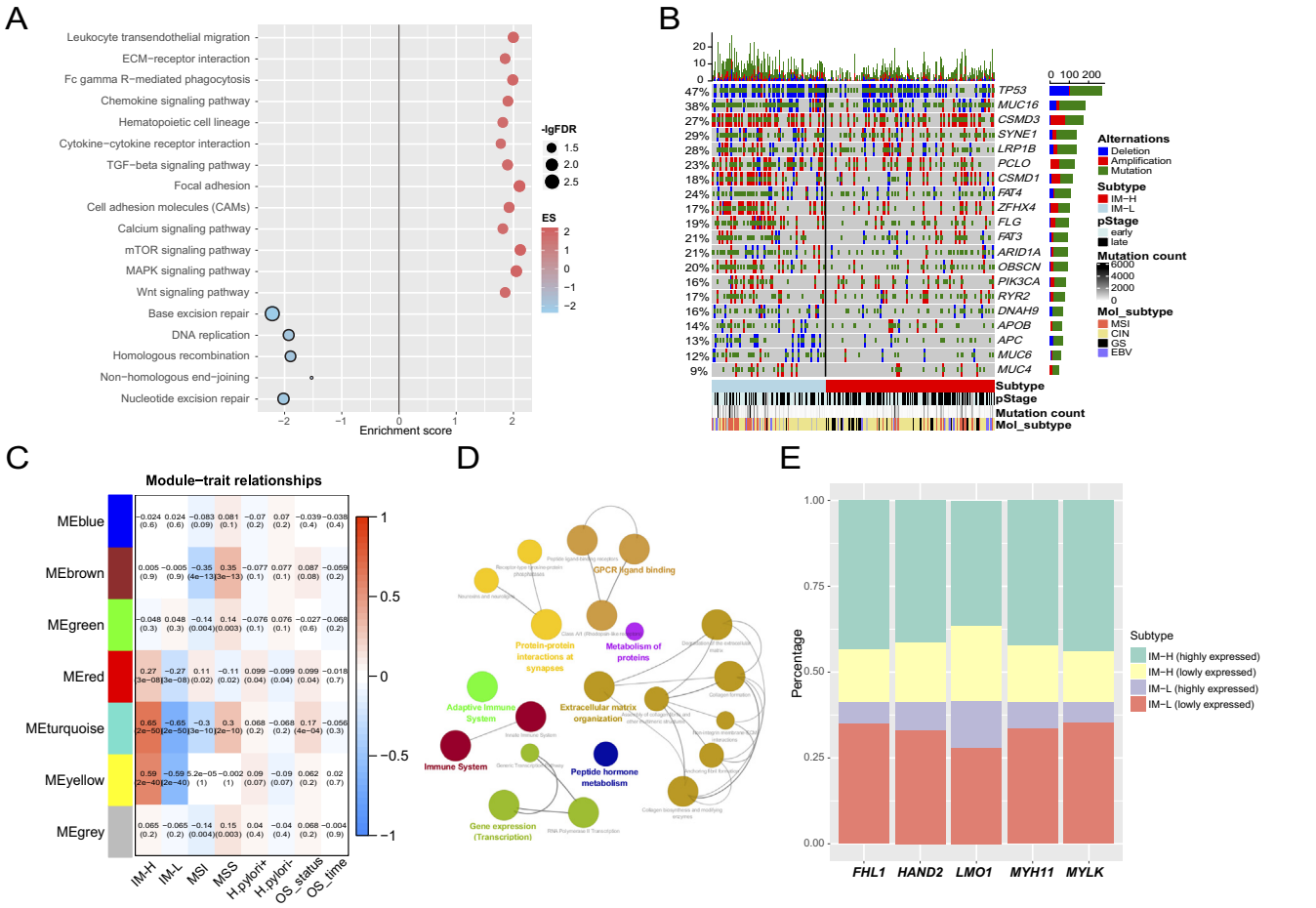

Fig. 3. Identification of IM-H and IM-L subtype-specific pathways, genomic, clinical features, gene ontology, and networks. **A.** KEGG pathways enriched in IM-H and IM-L. **B.** Mutation heatmap showed distribution of highly variant mutated genes, the genome and clinical molecular feature difference between IM-H and IM-L subtypes. **C.** Gene modules significantly differentiating GC by subtype, microsatellite status, *H. pylori* infection status, and survival time, or survival status. **D.** REACTOME pathways associated with genes in the MEturquoise module ($P < 0.05$). **E.** The expression distribution of key genes in the MEturquoise module in IM-H and IM-L subtypes.

in IM-L subtypes may be much higher than in IM-H. This indicates that the activities of these pathways could be negatively associated with GC immunity. In fact, our previous study has shown that the activity of MAPK pathways positively related with immune signatures, while the activity of the mismatch repair pathway negatively correlated with immune signatures in GC [30].

Identification of GC subtype-specific genomic and clinical features

In order to further distinguish the genomic differences between IM-H and IM-L, we first compared and identified the genes with high mutation rates (> 10%) in TCGA and ACRG datasets (Fig. 3B). The result showed that *TP53* had the highest mutation rate in GC, and has a significantly higher mutation rate in IM-L than in IM-H (Fisher's exact test, $P = 0.04$ (TCGA), $P = 0.12$ (ACRG)), which was consistent with our previous studies that *TP53* mutations inhibit tumor immunity in GC [30]. *MUC16* had the second highest mutation rate in GC and was also significantly higher in IM-L than in IM-H (Fisher's exact test, $P = 0.002$ (TCGA), $P = 0.04$ (ACRG)). In addition, there were several genes which were identified with a significantly higher mutation rate in IM-L than in IM-H, such as *ZFHX4*, *FAT3*, *FAT4* and *PCLO*. And there were some important genes such as *ARID1A* and *APC* (Fisher's exact test, $P = 0.004$ (*ARID1A*), $P = 0.001$ (*APC*)) were more frequently mutated in IM-L than in IM-H.

Furthermore, we compared somatic copy number alteration (SCNA) levels of important mutant genes between IM-H and IM-L subtypes (Fig. 3B). The result showed that *TP53* had significantly copy number deletion in both IM-H and IM-L, and the copy number deletion was markedly higher in IM-L subtype than in IM-H subtype (Fisher's exact test, $P = 0.008$). Other genes such as *SYNE1*□*APC* and *PCLO* were also showed significantly copy number deletion in IM-L subtype ($P < 0.05$). Moreover, some genes such as *CSMD1*, *OBSCN*, *ZFHX4*, *FLG* and *PCLO* were frequently amplified in IM-L subtypes ($P < 0.05$). These results demonstrated that IM-L subtype has a much higher frequency of genomic instability, in addition to the higher mutation frequency.

Then we further compared the differences of clinical features between IM-H and IM-L (Fig. 3B), including pathological stage (pStage) and *Helicobacter pylori* (*H. pylori*) infection status, and four molecular subtypes of gastric cancer in TCGA: genomic stable (GS), chromosomal unstable (CIN), EB virus subtype (EBV) and microsatellite unstable (MSI). The results suggested that there was no statistical significance between GC subtypes and *H. pylori* infection status (Fisher's exact test, $P = 0.10$ (TCGA), $P = 0.20$ (ACRG)). In addition, there were more patients in advanced stage (pStage was “stage iii/iv”) in IM-H subtype than patients in IM-L subtype (Fisher's exact test, $P = 0.003$ (TCGA), $P = 1.11e\text{-}5$ (ACRG)). As most patients with advanced stage were associated with poor prognosis in IM-H subtype, which was consistent with previous survival analysis. Among the four molecular subtypes, EBV subtype had no obvious difference between IM-H and IM-L subtype. Nevertheless, the GS subtype have a significantly higher proportion in IM-H (Fisher's exact test, $P = 5.95e\text{-}9$ (TCGA), $P = 9.05e\text{-}7$ (ACRG)), while the CIN and MSI subtype has a higher proportion in IM-L (Fisher's exact test, $P = 0.001$ (CIN, ACRG), and $P = 3.12e\text{-}4$ (MSI, TCGA), $P = 0.001$ (MSI, ACRG). These results implied that the genome in IM-H is more stable than in IM-L, the mutations and copy number alterations are more frequent, and the MSI molecular subtype is much denser in IM-L, which is related to better immunotherapy response. In

contrast, patients with advanced stage were mainly in IM-H subtype, which had higher genomic stability, and thus had worse clinical prognosis.

Identification of GC subtype-specific gene ontology and networks

We then performed a weighted gene co-expression network analysis of these two datasets by WGCNA [24] and identified a series of gene modules (gene ontology) associated with the genes which were highly expressed. We found several gene modules that significantly differentiated GC by subtype, microsatellite status, *H. pylori* infection status, or survival time and survival status in TCGA (Fig. 3C). According to the modules relusts, the MEturquoise module was markedly elevated in IM-H (P = 2.0e-50, R = 0.65), while was depressed in IM-L (P = 2.0e-50, R = −0.65). Moreover, a high expressed MEturquoise module was associated with a worse survival prognosis in GC patients (P = 4.0e-4, R = 0.17). In addition, this module was negatively correlated with MSI (P = 3.0e-10, R = −0.3), and positively correlated with MSS (P = 2.0e-10, R = 0.3). In ACRG, the MEturquoise module has the highest correlation with various traits, and the trend is highly consistent with the results in TCGA. Then, we imported all of the genes in MEturquoise module into Cytoscape and perform pathway analysis. By screening the pathways with the number of genes more than 10 and $P < 0.05$, we found that the pathways which were significantly correlated with the MEturquoise module were mainly metabolism-related pathways (metabolism of proteins and peptide hormone metabolism), immune-related pathways (immune system, innate immune system and adaptive immune system), cell signaling pathways and extracellular matrix pathways (Fig. 3D).

We extracted and analyzed all the genes in the MEturquoise module (Supplementary materials, Table S4, Fig. S1,), and selected the key genes of the module by setting a weight threshold of 0.38, and finally identified 44 hub genes, including three transcription factor (TF) genes (*HAND2, FHL1, LMO1*), two oncogenes (*MYH11 and LMO1*), and a protease-related gene (*MYLK*), where *LMO1* is not only a transcription factor but an oncogene. To further study the relationship between these five key genes and immune subtypes, we compared the relationship between the expression level of these five genes and two immune subtypes. The results showed that the patients with high expression of these genes were accounted for a significantly higher proportion in the IM-H subtype (Fisher's exact test, P = 6.21e-25 (*HAND2*), 1.53e-33 (*FHL1*), 3.21e-9 (*LMO1*), 5.71e-28 (*MYH11*), 5.84e-36 (*MYLK*)) (Fig. 3E).

Class prediction of GC subtypes based on immune-related genes profiling

In order to verify the reliability and accuracy of the classification performance, we first constructed a deep neural network with TCGA dataset as the training set, ACRG and another gastric cancer dataset as the verification set. The results showed that the model accuracy was about 90% in the TCGA training dataset and 91% in the ACRG test dataset(Fig. 4A). We then predicted the GSE15459 dataset separately and divided 192 patients into two types: IM-H and IM-L. The ESTIMATE results showed that IM-H subtype had a significantly higher immune score and IM-L subtype had a significantly lower immune score (Mann-Whitney U test, P = 1.47e-12, Fig. 4B). Then we compared the clinical outcomes between IM-H and IM-L patients in GSE15459 after prediction, and we found that IM-H subtype which was predicted based on the deep neural network model had a worse survival prognosis than the predicted IM-L subtype (P = 0.045, Fig. 4C). In addition, we used random forest (RF) and Naïve Bayesian models for the same training to compare the performance of other classifiers in the weka library. The results showed that in the random forest model, the accuracy of the training dataset (TCGA) and the test dataset (ACRG) were 92% and 79%, and in the naive Bayes model the accuracy were 90% and 77% (Fig. 4A). Compared the above results, the deep neural network model has significantly higher accuracy than the other two commonly used models in the Weka library, but the overall model accuracy is relatively high, suggesting that the characteristic value used for classification in this experiment can be applied to many different datasets, and had universal applicability. These results demonstrate that the immunogenomic profiling-based classification of GC is stable and predictable.

Discussion

A number of prior studies have identified GC subtypes on the basis of genomic profiling [6,7]. However, very few studies have investigated the classification based on immune risk genes and verified the reliability and accuracy of the classification. To fill the gaps in knowledge of GC, we focused on identifying immune-related GC subtypes using immune-related genes that were screened significantly related to prognosis through a risk regression model, and identified the subtype-specific clinical features and molecular characters (Fig. 5). Our results show that GC could be classified into two stable subtypes: IM-H and IM-L. Moreover, we confirmed that this classification was duplicable and predictable. The IM-H GC subtype was enriched not only in immune signatures, but also in many cancer-associated pathways including TGF-beta signaling pathway, Focal adhesion, Cell adhesion molecules (CAMs), Calcium signaling pathway, mTOR signaling pathway, MAPK signaling pathway and Wnt signaling pathway (Fig. 3A). This is in accordance with our previous study showing that various immune signatures positively correlated with the MAPK, focal adhesion and Calcium signaling pathways in GC [30]. In contrast, the IM-L GC subtype was impoverished in immune signatures but enriched in base excision repair, DNA replication, homologous recombination, non-homologous end-joining and nucleotide excision repair (Fig. 3A). It is reasonable that the

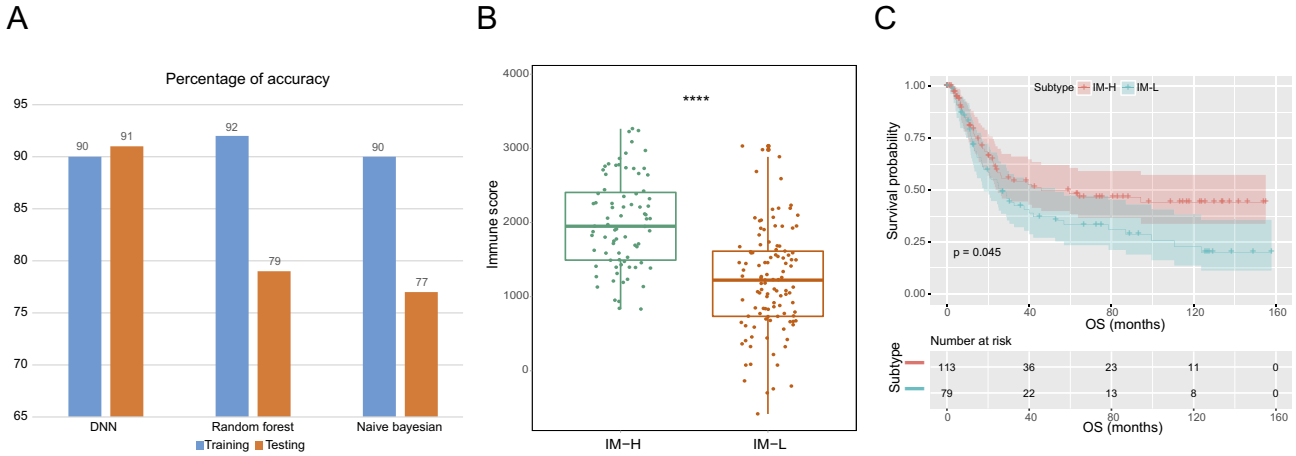

Fig. 4. Machine learning approach predicts GC phenotypes. **A.** Performance in the classification of TNBC subtypes based on immune signatures. **B.** Comparison of immune score of IM-H and IM-L subtype in the dataset GSE15459 predicted by the DNN model. *: P < 0.05, **: P < 0.01, ***: P < 0.001, ****: P < 0.0001. **C.** IM-H had a worse survival prognosis while IM-L had a better survival prognosis in GSE15459 dataset predicted by DNN model.

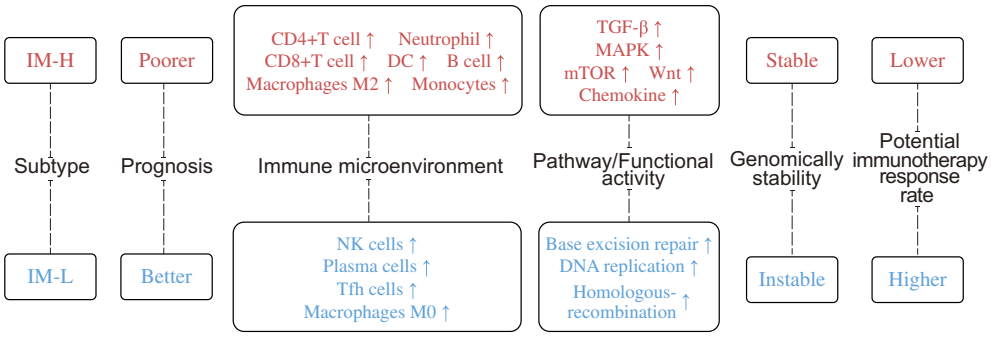

Fig. 5. A summary figure showed the proposed correlations between the molecular characterization, potential immunotherapy responsiveness and their identified immunogenomic profiling of GC.

mismatch repair pathway activity was negatively correlated with immune activity in cancer, as deficient mismatch repair often results in elevated tumor immunity [31]. Strikingly, we found that the cell cycle and pyrimidine metabolism signaling pathway were enriched in IM-L subtype GC. This observation is in line with previous studies that cell cycle inhibitors increase tumor immunogenicity [32]. Overall, these findings showed potential positive or negative associations between signaling pathways activities and immune activities in GC.

IM-H had significantly stronger immune cell infiltration and immune activities. e.g. higher immune score and stroma score (Fig. 1C). When we used TIMER to calculate the density of immune cell subsets in GC, we found that B cells, CD8 T cells, CD4 T cells, Neutrophil cells, Macrophages and Dendritic cells tended to be present in significantly higher numbers in IM-H than in IM-L (Mann–Whitney *U* test, $P < 0.05$) (Fig. 2C). This finding confirmed elevated tumor immune activity in IM-H. TMB has been associated with clinical response to immunotherapy [12]. Gene mutations may yield neoepitopes that can be recognized by immune cells [33] and were associated with antitumor immune response [10]. Several cancer types with high TMB have shown positive response to immune checkpoint blockade treatment [34], then we compared TMB between IM-H and IM-L in TCGA, and found that IM-L had higher TMB than IM-H (Mann-Whitney U test, $P = 1.78e\text{-}09$). This suggests that the differential immunogenicity between the GC subtypes can be attributed to TMB and neoantigens. The correlations of TMB with immune cell activities and function in GC should be elucidated in future studies.

Furthermore, we found higher clonal heterogeneity in IM-L, as estimated by ABSOLUTE [20], than in IM-H (Fig. 1C). Consistent with previous studies, clonal heterogeneity was shown to have a significant negative correlation with tumor immunity [35]. We further compared SCNA levels of important mutant genes between IM-H and IM-L subtypes (Fig. 3B). We found several genes showed frequently amplified or deleted in IM-L subtype, suggesting that IM-L subtype has a much higher frequency of genomic instability, such as MUC 16, *FAT3*, *FAT4*, and *PCLO*. Studies have shown that patients with *MUC16* mutations were associated with a better prognosis in GC, and had potential value for predicting anti-PD-1 therapy [36], which was consistent with our findings that IM-L has a better prognosis than IM-H. Besides, the lower expression of *FAT3* and *FAT4* genes is associated with worse overall survival in GC [37], and the inactivation of *PCLO* significantly promotes the migration of cancer cells in liver cancer [38]. These findings demonstrated that IM-H had lower levels of SCNAs compared to IM-L, supporting the notion that high tumor aneuploidy correlates with reduced tumor immune infiltration [39].

Furthermore, we compared the differences of clinical characters between IM-H and IM-L subtype. Our findings showed that GS subtype had a significantly higher proportion in IM-H while CIN and MSI subtype had a significantly higher proportion in IM-L. Chromosomal instability has a strong correlation with tumor immunotherapy response [40], and microsatellite instability status could be as additional predictive biomarker of response to immunotherapy. These results suggested that IM-L may have a better immunotherapy response than IM-H.

In addition, we extracted and analyzed all the genes in the MEturquoise module and found five important genes (*HAND2*, *LMO1*, *MYH11*, *MYLK* and *FHL1*) which accounted for a significantly higher proportion in the IM-H subtype. *HAND2* can regulates interleukin 15 (IL15), a key immune factor required for the activation and survival of uterine natural killer (uNK) cells [41]. *LMO1* overexpression in GC could be as one of new markers of poor prognosis [42]. The proteins encoded by *MYH11* were upregulated in node-positive GC tissues [43]. *MYLK* overexpression in stroma cells may regulate GC cells proliferation, apoptosis, invasion and migration [44]. Most of these findings were consistent with results from previous studies. The contradiction was that the patients with low *FHL1* expression tumor showed significantly shorter survival ($P < 0.05$) than those with high *FHL1* expression tumors [45]. It might be related to the microenvironment of the two subtypes, and further research is needed.

Presently, immunotherapy for GC is an active area of investigation [46]. However, some preliminary immunotherapy clinical trials have not shown significant improvement in GC patients (personal communication). Thus, the classification of GC based on the immune signature may help to stratify GC patients to identify those who respond to immunotherapy. It is conceivable that patients with an IM-H subtype of GC would be more likely to respond to anti-CTLA4 treatment than patients with IM-L subtype, since *CTLA4* is more highly expressed in IM-H GC (Mann-Whitney *U* test $P = 1.29e\text{-}8$ (TCGA) $P = 0.0035$ (ACRG), and *CTLA4* expression would be a predictive biomarker for the response to CTLA4-directed immunotherapy.

Conclusions

We proposed and validated two reproducible immune molecular subtypes of GC, which has potential clinical implications for GC patient selection of immunotherapy. In addition, TMB may be associated with immune activities in GC.

Supplementary data to this article can be found online at https://doi.org/10.1016/j.tranon.2020.100888.

Funding support

This work was supported by Social development project of Jiangsu Science and Technology Department (BE2019758). and Six Talent Peak in Jiangsu Province(TD-SWYY-007).

CRediT authorship contribution statement

Zhixian Liu: Conceptualization, Methodology, Software, Writing-Original draft preparation. Zehang Jiang: Data curation, Methodology, Software, Writing- Original draft preparation. Nan Wu: Visualization, Investigation. Xiaosheng Wang: Conceptualization, Resources. Guoren Zhou: Conceptualization, Funding acquisition, Writing-Reviewing and Editing.

Declaration of competing interest

The authors declare that they have no known competing financial interests or personal relationships that could have appeared to influence the work reported in this paper.

References

[1] F. Bray, J. Ferlay, I. Soerjomataram, et al., Global cancer statistics 2018: GLOBOCAN estimates of incidence and mortality worldwide for 36 cancers in 185 countries [J], CA Cancer J. Clin. 68 (6) (2018) 394–424.

[2] R.M. Feng, Y.N. Zong, S.M. Cao, et al., Current cancer situation in China: Good or bad news from the 2018 Global Cancer Statistics? [J], Cancer Commun (Lond) 39 (1) (2019) 22.

[3] N. Cancer Genome Atlas Research. Comprehensive molecular characterization of gastric adenocarcinoma [J]. Nature, 2014. 513(7517): p. 202–9.

[4] R. Cristescu, J. Lee, M. Nebozhyn, et al., Molecular analysis of gastric cancer identifies subtypes associated with distinct clinical outcomes [J], Nat. Med. 21 (5) (2015) 449–456.

[5] T. Chen, X.Y. Xu, P.H. Zhou, Emerging molecular classifications and therapeutic implications for gastric cancer [J], Chin J Cancer 35 (2016) 49.

[6] Y.J. Zhou, G.Q. Zhu, X.F. Lu, et al., Identification and validation of tumour microenvironment-based immune molecular subgroups for gastric cancer: Immunotherapeutic implications [J], Cancer Immunol Immunother 69 (6) (2020) 1057–1069.

[7] D. Zeng, M. Li, R. Zhou, et al., Tumor microenvironment characterization in gastric cancer identifies prognostic and immunotherapeutically relevant gene signatures [J], Cancer Immunol Res 7 (5) (2019) 737–750.

[8] J.C. Del Paggio, Immunotherapy: Cancer immunotherapy and the value of cure [J], Nat. Rev. Clin. Oncol. 15 (5) (2018) 268–270.

[9] X. Li, C. Shao, Y. Shi, et al., Lessons learned from the blockade of immune checkpoints in cancer immunotherapy [J], J. Hematol. Oncol. 11 (1) (2018) 31.

[10] D.A. Braun, K.P. Burke, E.M. Van Allen, Genomic approaches to understanding response and resistance to immunotherapy [J], Clin. Cancer Res. 22 (23) (2016) 5642–5650.

[11] A. Snyder, V. Makarov, T. Merghoub, et al., Genetic basis for clinical response to CTLA-4 blockade in melanoma [J], N. Engl. J. Med. 371 (23) (2014) 2189–2199.

[12] N.A. Rizvi, M.D. Hellmann, A. Snyder, et al. Cancer immunology. Mutational landscape determines sensitivity to PD-1 blockade in non-small cell lung cancer [J]. Science, 2015. 348(6230): p. 124–8.

[13] W. Hugo, J.M. Zaretsky, L. Sun, et al., Genomic and Transcriptomic features of response to anti-PD-1 therapy in metastatic melanoma [J], Cell 168 (3) (2017) 542.

[14] E.M. Van Allen, D. Miao, B. Schilling, et al., Genomic correlates of response to CTLA-4 blockade in metastatic melanoma [J], Science 350 (6257) (2015) 207–211.

[15] D.T. Le, J.N. Uram, H. Wang, et al., PD-1 blockade in tumors with mismatch-repair deficiency [J], N. Engl. J. Med. 372 (26) (2015) 2509–2520.

[16] G. Bindea, B. Mlecnik, M. Tosolini, et al., Spatiotemporal dynamics of intratumoral immune cells reveal the immune landscape in human cancer [J], Immunity 39 (4) (2013) 782–795.

[17] K. Yoshihara, M. Shahmoradgoli, E. Martinez, et al., Inferring tumour purity and stromal and immune cell admixture from expression data [J], Nat. Commun. 4 (2013) 2612.

[18] T. Li, J. Fan, B. Wang, et al., TIMER: A web server for comprehensive analysis of tumor-infiltrating immune cells [J], Cancer Res. 77 (21) (2017) e108–e110.

[19] A.M. Newman, C.L. Liu, M.R. Green, et al., Robust enumeration of cell subsets from tissue expression profiles [J], Nat. Methods 12 (5) (2015) 453–457.

[20] S.L. Carter, K. Cibulskis, E. Helman, et al., Absolute quantification of somatic DNA alterations in human cancer [J], Nat. Biotechnol. 30 (5) (2012) 413–421.

[21] P. Van Loo, S.H. Nordgard, O.C. Lingjaerde, et al., Allele-specific copy number analysis of tumors [J], Proc. Natl. Acad. Sci. U. S. A. 107 (39) (2010) 16910–16915.

[22] A. Subramanian, P. Tamayo, V.K. Mootha, et al., Gene set enrichment analysis: A knowledge-based approach for interpreting genome-wide expression profiles [J], Proc. Natl. Acad. Sci. U. S. A. 102 (43) (2005) 15545–15550.

[23] C.H. Mermel, S.E. Schumacher, B. Hill, et al. GISTIC2.0 facilitates sensitive and confident localization of the targets of focal somatic copy-number alteration in human cancers [J]. Genome Biol, 2011. 12(4): p. R41.

[24] P. Langfelder, S. Horvath, WGCNA: An R package for weighted correlation network analysis [J], BMC Bioinformatics 9 (2008) 559.

[25] G. Bindea, B. Mlecnik, H. Hackl, et al., ClueGO: A cytoscape plug-in to decipher functionally grouped gene ontology and pathway annotation networks [J], Bioinformatics 25 (8) (2009) 1091–1093.

[26] G. Bindea, J. Galon, B. Mlecnik, CluePedia cytoscape plugin: pathway insights using integrated experimental and in silico data [J], Bioinformatics 29 (5) (2013) 661–663.

[27] J.A. Thompson, J. Tan, C.S. Greene, Cross-platform normalization of microarray and RNA-seq data for machine learning applications [J], PeerJ 4 (2016), e1621, .

[28] K. Chaudhary, O.B. Poirion, L. Lu, et al., Deep learning-based multi-omics integration robustly predicts survival in liver cancer [J], Clin. Cancer Res. 24 (6) (2018) 1248–1259.

[29] M. Kanehisa, M. Furumichi, M. Tanabe, et al., KEGG: New perspectives on genomes, pathways, diseases and drugs [J], Nucleic Acids Res. 45 (D1) (2017) D353–D361.

[30] Z. Jiang, Z. Liu, M. Li, et al., Immunogenomics analysis reveals that TP53 mutations inhibit tumor immunity in gastric cancer [J], Transl. Oncol. 11 (5) (2018) 1171–1187.

[31] D.T. Le, J.N. Durham, K.N. Smith, et al., Mismatch repair deficiency predicts response of solid tumors to PD-1 blockade [J], Science 357 (6349) (2017) 409–413.

[32] S. Goel, M.J. DeCristo, A.C. Watt, et al., CDK4/6 inhibition triggers anti-tumour immunity [J], Nature 548 (7668) (2017) 471–475.

[33] E.F. Fritsch, N. Hacohen, C.J. Wu, Personal neoantigen cancer vaccines: the momentum builds [J], Oncoimmunology 3 (2014), e29311, .

[34] J. Larkin, V. Chiarion-Sileni, R. Gonzalez, et al., Combined nivolumab and ipilimumab or monotherapy in untreated melanoma [J], N. Engl. J. Med. 373 (1) (2015) 23–34.

[35] V. Thorsson, D.L. Gibbs, S.D. Brown, et al., The immune landscape of cancer [J], Immunity 51 (2) (2019) 411–412.

[36] E.C. Smyth, R.C. Fitzgerald, MUC16 mutations and prognosis in gastric cancer: A little Goes a long way [J], JAMA Oncol 4 (12) (2018) 1698–1699.

[37] X. Jiang, Z. Liu, Y. Xia, et al., Low FAT4 expression is associated with a poor prognosis in gastric cancer patients [J], Oncotarget 9 (4) (2018) 5137–5154.

[38] A. Fujimoto, M. Furuta, Y. Shiraishi, et al., Whole-genome mutational landscape of liver cancers displaying biliary phenotype reveals hepatitis impact and molecular diversity [J], Nat. Commun. 6 (2015) 6120.

[39] T. Davoli, H. Uno, E.C. Wooten, et al. Tumor aneuploidy correlates with markers of immune evasion and with reduced response to immunotherapy [J]. Science, 2017. 355 (6322).

[40] K.W. Mouw, M.S. Goldberg, P.A. Konstantinopoulos, et al., DNA damage and repair biomarkers of immunotherapy response [J], Cancer Discov 7 (7) (2017) 675–693.

[41] H. Murata, S. Tanaka, T. Tsuzuki-Nakao, et al., The transcription factor HAND2 upregulates transcription of the IL15 gene in human endometrial stromal cells [J], J. Biol. Chem. 295 (28) (2020) 9596–9605.

[42] Y. Sun, G.J. Ma, X.J. Hu, et al., Clinical significance of LMO1 in gastric cancer tissue and its association with apoptosis of cancer cells [J], Oncol. Lett. 14 (6) (2017) 6511–6518.

[43] Y. Ma, Y.F. Li, T. Wang, et al., Identification of proteins associated with lymph node metastasis of gastric cancer [J], J. Cancer Res. Clin. Oncol. 140 (10) (2014) 1739–1749.

[44] L. Chen, L. Su, J. Li, et al., Hypermethylated FAM5C and MYLK in serum as diagnosis and pre-warning markers for gastric cancer [J], Dis. Markers 32 (3) (2012) 195–202.

[45] Y. Xu, Z. Liu, K. Guo, Expression of FHL1 in gastric cancer tissue and its correlation with the invasion and metastasis of gastric cancer [J], Mol. Cell. Biochem. 363 (1–2) (2012) 93–99.

[46] D. Vrana, M. Matzenauer, C. Neoral, et al. From tumor immunology to Immunotherapy in gastric and esophageal cancer [J]. Int. J. Mol. Sci., 2018. 20(1).